Environmental and Experimental Botany 221 (2024) 105713

Contents lists available at ScienceDirect

Environmental and Experimental Botany

journal homepage: www.elsevier.com/locate/envexpbot

Research Paper

Ca-oxalate crystals are involved in cadmium storage in a high Cd accumulating cultivar of cacao

Hester Blommaert [a,*], Hiram Castillo-Michel [b], Giulia Veronesi [c], Rémi Tucoulou [b], Jacques Beauchêne [d], Pathmanathan Umaharan [e], Erik Smolders [f], Géraldine Sarret [a,*]

[a] Université Grenoble Alpes, Université Savoie Mont Blanc, CNRS, IRD, Université G. Eiffel, ISTerre, Grenoble, France
[b] ESRF, The European Synchrotron, CS 40220, Grenoble Cedex 9 38043, France
[c] Université Grenoble Alpes, CNRS, CEA, IRIG, Laboratoire de Chimie et Biologie des Métaux, 17 rue des Martyrs, Grenoble 38000, France
[d] CIRAD, UMR Ecologie des Forêts de Guyane (EcoFoG), AgroParisTech, CNRS, INRA, Université des Antilles, Université de Guyane, Kourou 97310, France
[e] Cocoa Research Centre, University of the West Indies, St. Augustine, Trinidad and Tobago
[f] Division of Soil and Water Management, Department of Earth and Environmental Sciences, KU Leuven, Belgium

ARTICLE INFO

Keywords:
Ca-oxalate
Distribution
Imaging
Metal pathways
O-ligands
S-ligands
Speciation
Synchrotron
Theobroma cacao L
X-Ray absorption spectroscopy

ABSTRACT

Cadmium (Cd) concentrations in cacao often exceed food limits. A better understanding of the molecular mechanisms of Cd accumulation in cacao trees is necessary to advance Cd mitigation strategies. This study explores Cd distribution and speciation (i.e., chemical form) within the vegetative organs of a high Cd accumulating cacao cultivar growing in soil with background Cd concentrations (0.28 mg Cd kg^{-1}) by synchrotron radiation-based micro- and nano-X-ray fluorescence imaging and X-ray absorption spectroscopy on duplicate samples of roots, young branches, mature branches, and leaves. In both the roots and branches, the incorporation of Cd in Ca-oxalate crystals with binding to oxygen-ligands was identified as a major mechanism of Cd regulation. The Ca-oxalate crystals were more abundant in the branches than in the roots. We suggest that the incorporation of Cd into the Ca-oxalate crystals may limit the transfer of Cd to other organs like the leaves and beans. The roots also featured Cd-sulfur species in dilated cells of the wood, probably for the retention of Cd in the roots by strong binding with Cd to thiol-containing ligands. A Cd hotspot in large, secreting channels of the branches suggested that mucilage may play a role in the transport of Cd within cacao trees. The leaves had local Cd enrichments in the parenchymatous tissues and displayed a higher Cd concentration in the mesophyll compared to the epidermis. These insights in Cd distribution and speciation underscore that *Theobroma cacao* L. develops original Cd detoxification strategies, strongly different from non-tolerant species such as cereals.

1. Introduction

Cadmium (Cd) is a non-essential trace metal that is highly toxic to most living organisms (Sigel et al., 2013). The metal has been related to adverse health effects in humans upon chronic exposure (FAO/WHO, 2010). To protect consumers, regulatory bodies have imposed strict limits on maximal Cd concentrations in food. While regulations originally focused on main food items contributing to Cd exposure such as rice, wheat and potatoes, more recent regulation now also include chocolate and cacao powders with limits set between 0.10 and 0.80 mg Cd kg^{-1} (Australia New Zealand Food Standards Code, 2017; Codex Alimentarius Commission, 2018; EU, 2014; Mercosur, 2011; Ministry of Health of the Russian Federation, 2011). Cacao is a moderate Cd accumulator and young soils naturally have high Cd concentrations leading to widespread exceedances of the limits in some regions. These regulations have fueled research worldwide to monitor and mitigate Cd accumulation in cacao (Meter et al., 2019; Vanderschueren et al., 2021). However, the molecular mechanisms underlying Cd accumulation in cacao trees remain elusive, hindering the development of Cd mitigation strategies.

Synchrotron-based X-ray absorption spectroscopy (XAS) and X-ray fluorescence (XRF) are non-destructive techniques that allow to measure

Abbreviations: XAS, X-Ray Absorption Spectroscopy; XRF, X-Ray fluorescence; LA-ICP-MS, Laser-Ablation inductively couples mass spectrometry; XANES, X-ray absorption near edge spectroscopy.

* Corresponding authors.
E-mail addresses: hester.blommaert@gmail.com (H. Blommaert), Geraldine.sarret@univ-grenoble-alpes.fr (G. Sarret).

https://doi.org/10.1016/j.envexpbot.2024.105713
Received 4 December 2023; Received in revised form 31 January 2024; Accepted 22 February 2024
Available online 24 February 2024

the *in vivo* chemical speciation of elements and their cellular localization (Kopittke et al., 2018; Zhao et al., 2014). This information can be used to elucidate how different cell types or tissue structures control the distribution, complexation, and storage of Cd. Yet, the use of these techniques is currently limited because of their relatively high detection limit compared to the Cd concentrations in plant organs when grown in soils with natural concentrations of Cd (0.01 – 1 mg Cd kg^{-1} DW) (Smolders and Mertens, 2013). As a consequence, most XAS and XRF plant studies are from contaminated environments or lab studies with plants suffering from high Cd exposure (see studies in reviews of Sarret et al., 2013; Zhao et al., 2014; Kopittke et al., 2018; Aucour et al., 2023). To the best of our knowledge, there are only few studies with speciation and/or localization data at low or background concentrations (Gu et al., 2020; Sari et al., 2022; Yan et al., 2020, 2022). The current literature on metal speciation and localization is thus biased towards plants that cope with high exposure levels of Cd.

The majority of the current knowledge regarding the molecular mechanisms of Cd accumulation in plants originates from studies on annual crops or hyperaccumulator plants (Clemens and Ma, 2016; McLaughlin et al., 2021; Sterckeman and Thomine, 2020), and is described briefly in this paragraph. Cadmium is in a first step taken up from the soil by root metal transporters for micronutrients. Once inside the root symplasm, Cd can be either sequestered or migrate towards the central cylinder and be loaded into the xylem (Clemens and Ma, 2016). Most studies on annual crops or non-tolerant species show that the plants have the tendency to sequester Cd in vacuoles of the roots, to limit the transfer to shoot tissues (excluder strategy), while hyperaccumulator species transfer Cd to aboveground tissues (van der Ent et al., 2013). Recent studies in rice and eggplant roots, suggested that most Cd in the roots is immobilized and stored as Cd-sulfur (S) complexes (Pons et al., 2021; Wiggenhauser et al., 2021a). These Cd-S complexes, can be molecules containing thiol groups such as glutathione, and phytochelatins (Clemens, 2019). Conversely, Cd hyperaccumulator plants tend to bind Cd in roots with mainly oxygen (O)-ligands (Vogel-Mikuš et al., 2010; Tian et al., 2011). Possible O-containing ligands described currently in literature are carboxyl/hydroxyl groups from cell-wall compounds and/or organic acids. Concentration measurements in mature cacao trees growing in environmental relevant conditions, indicated that the roots are a minor compartment for Cd accumulation, as most of the Cd is transported to the shoots (Blommaert et al., 2022; Engbersen et al., 2019). Isotope analysis in the first-mentioned study suggested moreover that a possible mechanism of retention in the root could be due to binding with S-ligands in the vacuole as observed in rice roots (Wiggenhauser, 2021 a). Yet, to date there are no measurements of the localization and chemical forms of Cd in cacao roots that confirm this hypothesis.

After loading into the root xylem of plants, Cd is further transported to the transpiring organs like leaves, via intermediate tissues like stems or branches. During the transport, Cd can interact and sorb on the cell wall of xylem vessels. Finally, Cd is unloaded into stem and leaf cells (Clemens and Ma, 2016; Sterckeman and Thomine, 2020). The Cd forms in the xylem have been described as both Cd-S and Cd-O species. In studies on hyperaccumulator plants, the main proportion of Cd was bound with O-ligands, probably provided by organic acids (Küpper et al., 2004; Tian et al., 2011). In eggplant, most Cd in the stems was bound to S-ligands in the stems (Pons et al., 2021). In rice, the speciation of Cd in the shoots changed from binding with S-ligands to binding with O-ligands upon maturation (Wiggenhauser, 2021b). By comparing the Cd speciation in the leaves of a hyperaccumulator, and a non-accumulator species, authors found that the degree of binding of Cd with O-ligands versus S-ligands, was actually associated with the tolerance the plant has towards Cd (Isaure et al., 2015). Along the same lines, a study on *Noccaea caerulescens* L. grown in a moderately contaminated soil, indicated that the proportional binding of Cd with organic acids (O-ligands) relative to S-ligands may become more important with increasing Cd exposure. However, the spectra were done on freeze-dried samples, which could have created artefacts (Yan et al., 2022). In general, there is little data on transient and storage forms in the stem/-branch tissue as this compartment is often not present or neglected in annual crops and hyperaccumulator herbaceous species. A previous study on a high Cd accumulating genotype of cacao highlighted that the branches were a main accumulation compartment for Cd (Blommaert et al., 2022). Imaging of the branches indicated moreover that most Cd accumulated in the bark, and more specifically in the phloem rays and the periderm of the branches, which were hypothesized to be a form of Cd storage. Speciation measurements showed that Cd was predominantly associated with oxygen (C)-ligands in the cacao branches. Plausible ligand candidates were ascribed to be the O- functional group of an organic ligand and/or cell wall components, as observed in Cd hyperaccumulating species like *Arabidopsis halleri* and *Sedum alfredii* (Huguet et al., 2012; Tian et al., 2017), however, more data is necessary to corroborate this hypothesis.

Once in the leaf cytosol, Cd can migrate via symplastic pathways between cells. To safeguard photosynthetic activity, Cd is preferentially stored in the epidermis for the majority of hyperaccumulators (Leitenmaier and Küpper, 2013). However, variations exist, with some species showing a preferential Cd accumulation in the photosynthetic active mesophyll (Isaure et al., 2015; Küpper et al., 2000; Tian et al., 2017). Part of Cd can be reallocated from leaves to other organs via the phloem (White and Ding, 2023). The extent to which there is reallocation, depends on the phloem mobility of Cd and differs among plant species (Page and Feller, 2015; Sterckeman and Thomine, 2020). In the case of cacao, a significant proportion of Cd accumulates in the leaves (Vanderschueren et al., 2021). Nevertheless, to date it remains unknown where Cd accumulates in cacao leaves and whether Cd is being reallocated to other tissues.

This study builds up on earlier investigations in a high Cd accumulator genotype of cacao (Blommaert et al., 2022). The goal of this study was to comprehensively investigate the micro- and nanoscale distribution of Cd in various vegetative organs at background Cd concentrations and identify the chemical forms in which Cd accumulates within these tissues. To accomplish this, we utilized microXRF and nanoXRF imaging in conjunction with Cd L_{III}-edge microXANES speciation analyses.

2. Materials and methods

2.1. Study overview

We investigated the cultivar NA 312 from the *Nanay* genetic group (Motamayor et al., 2008). We selected this cultivar because various organs were already characterized in terms of bulk Cd concentration, isotope composition, and speciation in a previous study (Blommaert et al., 2022). The cultivar NA 312 was identified as a high Cd accumulator based on Cd levels in beans and leaves in a previous study at the International Cocoa Genebank, Trinidad, (ICGT) (Lewis et al., 2018). The ICGT is home to a field cacao collection comprising approximately 2400 cacao cultivars. The soil in the plot was a clayey loam soil with a pH of 4.1 ± 0.1 (mean ± standard deviation of three replicates), and a total Cd concentration of 0.28 ± 0.05 mg kg^{-1} (determined by aqua regia + HF digestion), which is in the range of Cd naturally present in soils (0.1 – 1 mg Cd kg^{-1}) (Smolders and Mertens, 2013).

In brief, as in previous study, we focused on a single cultivar with three biological replicates (T2, T4, and T6, T=Tree). The numbers correspond to specific trees within the field plot (there were more than three trees present on the plot). These biological replicates were genetically identical trees. We analyzed roots, young branches, mature branches, and leaves. Due to the long acquisition times because of the low Cd concentrations in the organs, the spectroscopy analyses were finally limited to only two biological replicates (T4 and T6). An overview of the tissues sampled, their respective Cd concentrations as measured in Blommaert et al. (2022), and the techniques used to analyze them, is provided in Table 1.

Table 1
Overview of organs sampled, analyses performed, and sample preparation for the two different biological replicates studied (T4, and T6). The Cd concentration of the organs measured in Blommaert et al. (2022) is given for reference.

Organ	Analyses performed		Sample prep.	*Cd (mg kg^{-1} DW^{-1})*
	T4	T6		*Mean ± SD*
Roots	µXRF + µXANES	µXRF + µXANES	FH	*3.21 ± 0.87*
Young branches	µXRF + µXANES	µXRF	FH	
Mature branches	nXRF	nXRF	OD	*6.12 ± 0.44*
Leaves	µXRF	nXRF	FH/FD	*3.49 ± 1.12*

FH: frozen-hydrated, FD: freeze-dried, OD: oven-dried. µXRF: micro X-Ray Fluorescence imaging. XANES: X-Ray absorption near edge. nXRF: nano X-Ray Fluorescence imaging. Cd concentration (mg kg^{-1} DW^{-1}) measurements by ICP-MS. The mean and standard deviation (SD) was calculated based on the mean of 3 biological replicates (T2, T4, and T6). For more details on the measurement see Blommaert et al. (2022).

2.2. Synchrotron-radiation based spectroscopy analyses

2.2.1. MicroXRF imaging and Cd L_{III}-edge microXANES analyses

2.2.1.1. Sample preparation. In October 2023, we collected roots, branches, and leaves following the procedures outlined in Blommaert et al. (2022). It should be noted that the sampled branches were at an earlier developmental stage compared to those sampled in the prior study (Figure S1). We will henceforth refer to these newly collected branches as 'young branches'.

The freshly sampled root, young branch, and leaf tissues underwent a series of preparation steps (Figure S1). They were initially washed with distilled water to rinse of soil and dust particles. The roots were afterwards submerged in Na_2-EDTA (20 mM) solution for 20 minutes, and rinsed again with distilled water. Intact pieces of plant tissue were put in an OCT (Optimal Cutting Temperature) resin (Tissue-Tek® O.C.T. Compound (polyvinyl alcohol and carbowax)), to allow subsequent cryosectioning (Figure S1). These samples embedded in OCT were then rapidly frozen in isopentane to preserve their fresh state, following the method described by Castillo-Michel et al. (2017). The samples were shipped in a dry shipper filled with liquid N_2, and stored in the laboratory facilities at −80∘C. Just before the measurement, transversal thin sections were prepared by cryosectioning the small frozen plant tissues, embedded in OCT, with a cryomicrotome (Leica RM2265/LN22). One sample was sectioned into several 'twin' thin Sections (1–5 mm diameter; 20 µm thick). One twin thin section was used to capture microscope images with a binocular, while the other twin thin section was transferred to the sample holder of the scanning X-ray microscope.

2.2.1.2. Data acquisition and treatment. The µXRF and µXAS analyses were performed on the ID21 scanning X-ray microscope at the European Synchrotron Radiation Facility (ESRF, Grenoble, France) on transversal thin sections of roots, young branches, and leaves (Table 1). Samples were transferred to the sample holder immediately after cutting and kept frozen during measurement. The X-ray beam was monochromatized with a Si(111) double-crystal monochromator and focused using Kirkpatrick-Baez mirrors on the sample with a lateral resolution of 0.6 µm (V) x 0.8 µm (H). The incident energy of the photon beam was 3.55 keV. Measurements were done in vacuum and under cryogenic conditions (110 K) using a liquid N_2 passively cooled cryostat (Cotte et al., 2017). The fluorescence signal was collected with a Silicon Drift Diode (SDD) XRF detector (SGX Sensortech with an active area of 80 mm^2) and normalized by the incident photon intensity.

Because plants contain a large amount of potassium (K), the K K_α fluorescence emission line (3313.8 eV) overlaps the most intense Cd line, Cd $L_{\alpha1}$ (3133.7 eV). Consequently, phosphorus (P), sulfur (S), chloride (Cl), magnesium (Mg), strontium (Sr) and cadmium (Cd) maps were recorded using an incident energy below the absorption edge of potassium (3550 eV). Maps were obtained by scanning the samples with a 2 µm step and a counting time of 100 ms per point.

The hyperspectral images were analyzed with the PyMCA software package. XRF data were energy calibrated, normalized by the incoming photon flux, and batch-fitted to extract elemental distributions. However, with the model already implemented in the PyMCA software, it was not possible to fit two background contributions that interfered with the Cd $L\alpha_1$ emission peak. These contributions were attributed to the sample matrix and to the K inelastic scattering. Therefore, we adopted an *ad hoc* Cd fitting strategy that consists in the addition of three Gaussian contributions (see section 1.1 in SI, Figure S2 and S3). Finally, to allow a visual comparison between different maps, we fixed the maximum value of photon counts for each element as specified in each figure legend.

In a selection of Cd spots observed in the branches and roots, Cd L_{III}-edge XANES spectra were collected in fluorescence mode with a silicon drift detector (SDD) in the energy range 3530–3600 eV. Ten to fifty scans of 3 min each from different spots were averaged using the Orange data mining software (Demšar et al., 2013).

After averaging, calibrating in energy, and normalizing, the XANES spectra were treated by linear combination fits (LCFs) using a XAS software (Fastosh (Landrot, 2018)). A database of Cd reference spectra recorded previously (Isaure et al., 2006) containing Cd-O species (Cd-cell wall, Cd-malate, Cd-oxalate, and Cd-pectin), and Cd-S species (Cd-cysteine and Cd-glutathione) was used for linear combination fitting (Figure S4). Cd-cell wall was remeasured during the measurement to calibrate the samples on the previously recorded database. As additional standard, Cd-Ca-Oxalate (Cd-O) was measured and included in the database (Figure S4). LCF was performed by fitting the normalized XANES spectra in regions between −20 and 55 eV (around the absorption edge), using the database of Cd reference compounds. The R-factor (in %) ($= \sum[\mu_{exp} - \mu_{fit}]^2 / \sum[\mu_{exp}]^2$)*100 was used to assess the goodness of fit. For some spectra, in particular the noisiest ones, different combinations of reference compounds provided equal goodness-of-fit. The fits of one XANES spectrum were considered of equivalent quality if the R-factor increased < 10 % compared to the best fit. For these spectra, several fits are shown.

2.2.2. NanoXRF imaging

2.2.2.1. Sample preparation. Mature branches and leaves were subjected to high resolution imaging with hard X-rays at the ID16B beamline (ESRF) (Table 1). The measurements were conducted at room temperature on either oven-dried (branches) or freeze-dried tissues (leaves). Freeze-drying is known to preserve elemental distribution (van der Ent et al., 2018). Drying may alter the elemental distribution. Therefore, we only used the maps obtained on dried tissues to confirm the elemental distribution observed in frozen-hydrated tissues for structures where we do not expect elemental redistribution. An example are crystalline structures such as Ca-oxalate crystals. Leaf thin sections were prepared by cryosectioning frozen-hydrated leaf sections in OCT using a cryomicrotome (Figure S1). These sections were freeze-dried in a vacuum for 3–4 hours and then transferred to a dry cabinet for 10 minutes to warm before being placed on a glass slide with Kapton tape before measurement. Mature branches, which had previously been characterized by laser ablation inductively coupled ICP-MS in a prior study (Blommaert et al., 2022), were oven-dried, re-humidified, embedded in OCT-resin, and cut into transversal cross sections with a cryomicrotome (Figure S1). All thin sections were securely fixed between ultralene foils.

2.2.2.2. Data acquisition and treatment. High resolution maps were

recorded with a 50 nm beam size and with an incident photon energy of 26.9 keV (above the Cd K-edge). The beam was focused using Kirkpatrick-Baez mirrors down to 50 × 50 nm^2. Fluorescence emission from the sample was captured using two multi-element SDD arrays positioned at 13° from the sample. High resolution maps were recorded at room temperature by raster scanning the sample in the X-ray focal plane with 100 × 100 nm^2 step size and 500 ms dwell time/pixel.

The hyperspectral images were analyzed with the PyMCA software package. XRF data were energy calibrated, normalized by the incoming photon flux, dead-time corrected, and batch-fitted to extract elemental maps. No XANES data were recorded due to a high degree of radiation damage observed in several attempts under non-cryogenic conditions.

3. Results

3.1. Cadmium localization in branches

3.1.1. MicroXRF imaging

In the optical images of the frozen hydrated young branch thin sections (Fig. 1), we identified several tissues including the pith, wood, bark, cortex, and periderm (Angyalossy et al., 2016). In the pith, we observed large vessel structures (indicated by 'z', Fig. 1). Further, it was possible to distinguish between the phloem rays (indicated by 'x', Fig. 1), and the phloem vessels (indicated by 'y', Fig. 1). This distinction was made evident through the presence of dilated parenchymatous tissues in the rays (x) (Angyalossy et al., 2016).

Across all tissue types, including pith, wood, bark, cortex, and periderm, we observed the presence of Cd (Fig. 1). It should be noted that the cortex and periderm were only mapped in one biological replicate (T4) due to time-constraints. Cadmium-strontium (Sr) correlating hotspots were present in the pith, wood, bark, cortex, and periderm. Particularly, in the bark parenchymatous tissues of the rays (x) near the cambium region, there was an enrichment of these spots. In addition, in the pith there was a notable accumulation of Cd within large vessel structures (z).

3.1.2. NanoXRF imaging

In the oven-dried mature branch thin sections, we mapped regions in the periderm (Fig. 2), in the bark and cambium (Figure S5), and in the wood (Figure S6). Across all these regions, we consistently detected the presence of Cd. Calcium (Ca) and Sr were found to systemically colocalize within prismatic crystals and less crystalline structures (Figure S5 and S6). Cadmium colocalized irregularly with these crystals (Fig. 1, S5, and S6). In a similar manner, nickel, copper and manganese were sporadically incorporated within the crystals (Fig. 2, S5, and S6).

3.2. Cadmium localization in roots

In the optical images of the frozen hydrated thin sections of biological replicates T4 and T6, several tissues are visible, including the wood, bark, and periderm (Fig. 3). In proximity to the cambium, along the side of the wood (Fig. 3 A, R1), Cd was heterogeneously distributed, and located within dilated (i.e. elongated) cells. No co-localization with other analyzed elements was identified in this particular area. In the center of the wood (Fig. 3 B, R3), a cluster of Cd-Sr spots was observed parallel to the xylem rays. In the wood and bark of replicate T4, we did not observe the Ca-oxalate crystals. The distribution of Cd was diffuse in the wood (Fig. 3, R4). There was an accumulation of Cd, Sr, and Cl in proximity of the cambium (R5). In the bark, a strong co-localization between Cd and S was noted (Fig. 3 B, R6). Contrary to the branches, in the periderm of the roots of replicate T6, our XRF measurements did not reveal any presence of Cd (Fig. 3 C).

3.3. Cadmium localization in leaves

3.3.1. MicroXRF imaging

In the optical images of a secondary vein of a frozen-hydrated leaf, distinct leaf structures were visible: a vascular bundle (v.b, Fig. 4) containing a xylem and a phloem region, surrounded by parenchymatous cells (par) and collenchyma (co). In the leaf blade, the epidermis (ep) and the mesophyll (mes) could be distinguished (Viet Ha et al., 2016).

Cadmium was not detected in the vascular bundle (Fig. 4 A). In the parenchymatous cells (both inside and outside the vascular bundles), there were local enrichments of Cd, some of which correlated with Sr (Fig. 4 B). At the base of the collenchyma cells (co, Fig. 4 B), we observed hotspot of Cd. Yet, this enrichment was not consistently observed in all collenchyma cells. In the leaf blade, we noticed a Cd enrichment in the upper side of the mesophyll compared to the epidermis and lower side of the mesophyll (Fig. 4 C).

3.3.2. NanoXRF imaging

In the freeze-dried leaf thin sections, we mapped the epidermis and mesophyll (Figure S7). The results confirmed that Cd was present in the mesophyll, not in the epidermis. Numerous Ca crystals were found to accumulate within the mesophyll. None of the analyzed elements (Br, K, Cd, Mn, Ni, and Zn) were incorporated into these crystals in the leaves.

3.3.3. Cd speciation in branches and roots

Regions with high Cd signal were selected to study Cd speciation by recording Cd L_{III}-edge μXANES spectra (Fig. 5, Table 2). We distinguished between two major groups of ligands that bind Cd in plants; (i) O-ligands represented by the references of Cd-cell wall, Cd-malate, Cd-oxalate, and Cd-pectin, S-ligands represented by the references Cd-cysteine and Cd-glutathione (Figure S4). The Cd L_{III}-edge XANES spectra show a clear distinction between Cd-S and Cd-O species because the Cd-O species have a peak at 3539 eV (Fig. 5) (Pickering et al., 1999).

In the Cd-Sr spots in the branches around the cambium (B2, B3, B4), Cd was 100 % bound to O-ligands. The recorded spectra in the Cd-Sr spot B2, were noisy, and here the fits also indicated Cd-S as species (up to 50 %). Similarly, in the center of the roots (Fig. 3), the Cd-Sr spots were mostly bound to O-ligands (R3), with a minority bound to sulfur-ligands. Speciation measurements in a Cd-diffuse area in the wood revealed that Cd was entirely bound to S-ligands (Fig. 3, R1). In other non-crystalline structures of the roots (Fig. 3, R4, R5, and R6), Cd was primarily bound to O-ligands (85–100 %), with Cd-S as a minor species. Interestingly, despite a clear correlation between Cd and S in the bark of the roots, the predominant speciation remained Cd-O (R6). For the O-ligands, the best linear combination fits were obtained with reference spectra from Cd-cell wall, Cd-oxalate, and Cd-Ca-oxalate.

4. Discussion

4.1. Cadmium accumulation in branches: the role of Ca-oxalate crystals

In the mature branches, the recorded average Cd concentration was 6.12 ± 0.44 mg kg^{-1} (mean ± SD, n=3 biological replicates) (Blommaert et al., 2022). The branches were the organ with the highest Cd concentrations, underscoring their significance in Cd regulation within the tree.

The XRF maps in this study at micro-and nanoscale of both young and mature branches showed that Cd was primarily observed in the form of crystal-shaped structures (Figs. 1 and 2). We observed these structures in all branch structures (pith, wood, bark, cortex, and periderm). However, there was a particular enrichment in the phloem rays of the bark (Fig. 1, 'x') which was in line with the Cd accumulation that was observed in the phloem rays of mature branches by LA-ICP-MS (Blommaert et al., 2022). These crystalline structures were identified as calcium oxalate crystals based on i) their prismatic morphology and ii)

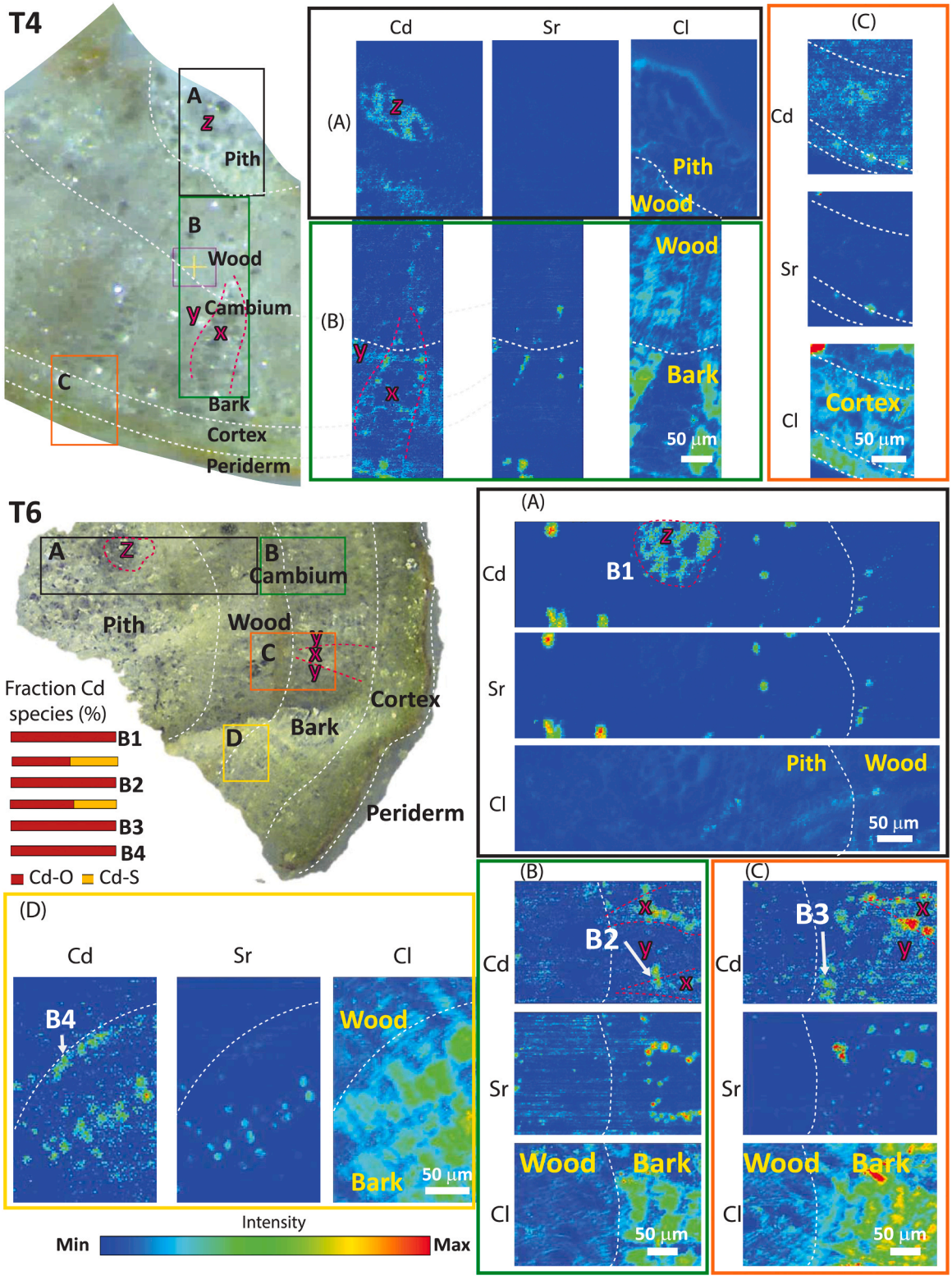

Fig. 1. Optical images of frozen-hydrated young branches of biological replicates T4 and T6 with the areas analyzed with µXRF (rectangles A, B, C, and D). The heatmaps show the distribution of Cd, Sr, and Cl in young branch tissues (pixel size: 1–2 µm). The color scale is adjusted to the range of each element (maximum photon counts: Cl: 10 000, Sr: 3000, Cd: 300). We distinguished between the phloem rays (x), phloem vessels (y) and the pith with large vessel structures (z).The Cl heatmaps are shown to visualize cellular structures. The Sr heatmaps are an indication for the presence of Ca-oxalate crystals. A strong colocalization between Sr and Cd was observed in all anatomical structures, and most pronounced in the bark, in proximity to the cambium (phloem rays (x)). In the pith, there was a notable Cd accumulation within a vessel structure (z). Spots B1, B2, B3, and B4 indicate the locations where Cd-XANES spectra were recorded (detailed spectra in Fig. 5). The results of linear combination fitting with Cd-O (red bar) and Cd-S (yellow bar) species are summarized in the bar diagram (% Cd species). Notably, Cd-O is the predominant speciation in the branches.

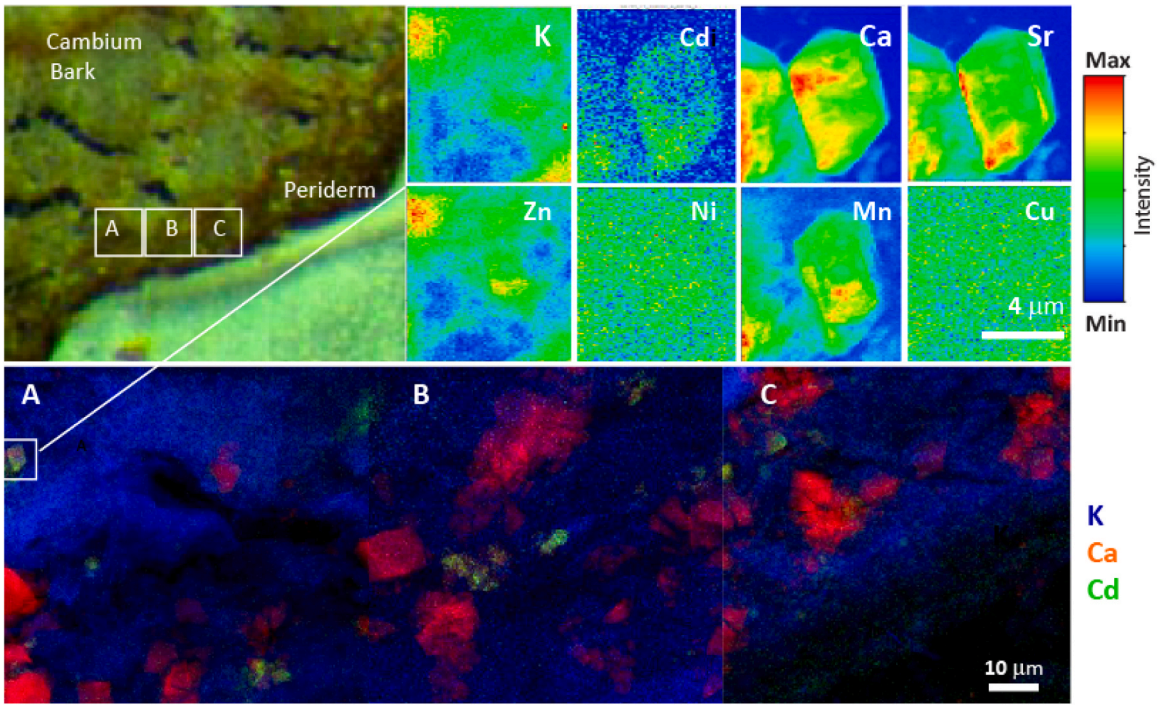

Fig. 2. Optical image of oven-dried mature branch of biological replicate T4 with the areas analyzed with nXRF (rectangles A, B, and C). RGB image showing the distribution of Ca (red), Cd (green), and K (blue). The heatmaps on the top right are the nXRF maps of K, Cd, Ca, Sr, Zn, Ni, Mn, and Cu at a twin prismatic oxalate crystal (pixel size 0.1 µm). The color scale is adjusted to the range of each element. K was displayed to show the cellular structure of the periderm area. Different forms of Ca-oxalate crystals are observed and in some of them, Cd was included. At the twin prismatic oxalate crystal, there was also an enrichment in Sr, Mn and Cd. Nickel, Zn and Cu were not observed within the crystal.

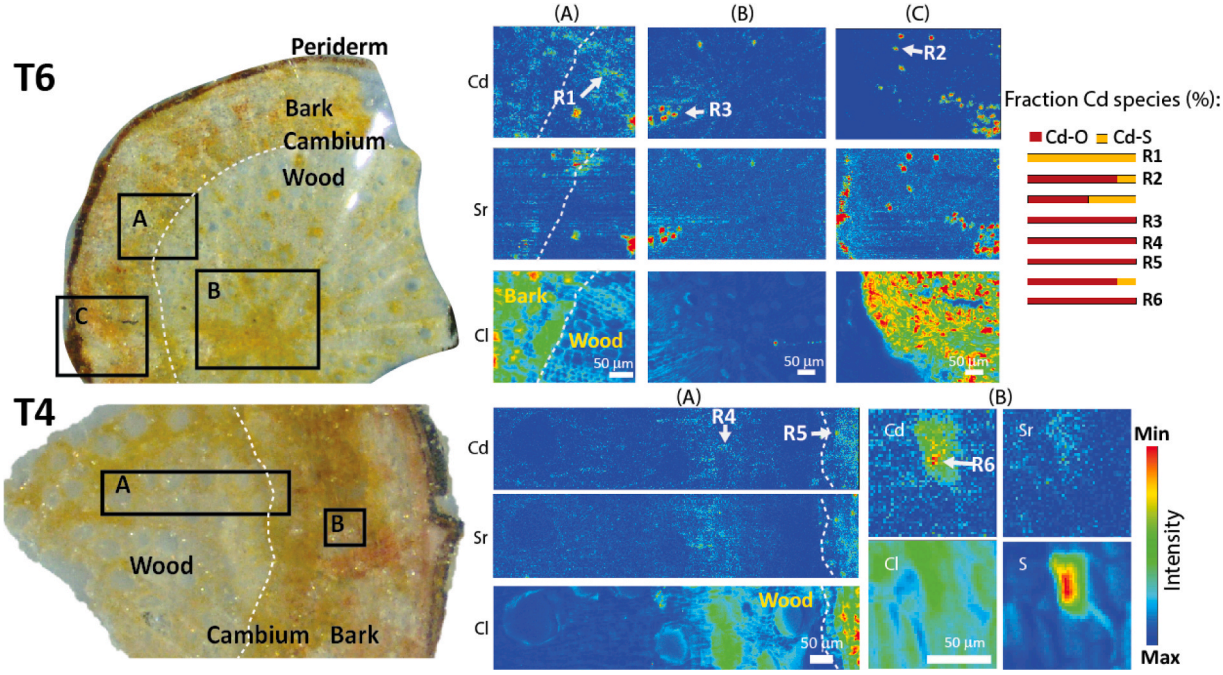

Fig. 3. Optical images of frozen-hydrated roots of biological replicates T4 and T6 with the areas analyzed with µXRF (rectangles A, B, C). The heatmaps show the distribution of Cd, Sr, and Cl (pixel size: 1–2 µm). The color scale is adjusted to the range of each element (maximum photon counts: Cl: 10 000, Sr: 3000, Cd: 300, S: 10 000). The Cl heatmaps are shown to visualize cellular structures. The Sr heatmaps are an indication for the presence of Ca-oxalate crystals. A strong colocalization between Sr and Cd was observed in the wood (R2 and R3). In proximity to the cambium, along the side of the wood (R1), Cd was located within dilated cells. In the bark, a Cd hotspot with a strong colocalization with S was noted (R6). Spots R1, R2, R3, R4, R5, and R6 indicate the locations where Cd-XANES spectra were recorded (detailed spectra in Fig. 5). The results of linear combination fitting with Cd-O (red bar) and Cd-S (yellow bar) species are summarized in the bar diagram (% Cd species). Cd-O is the predominant speciation in the roots, but also Cd-S species were observed (R1).

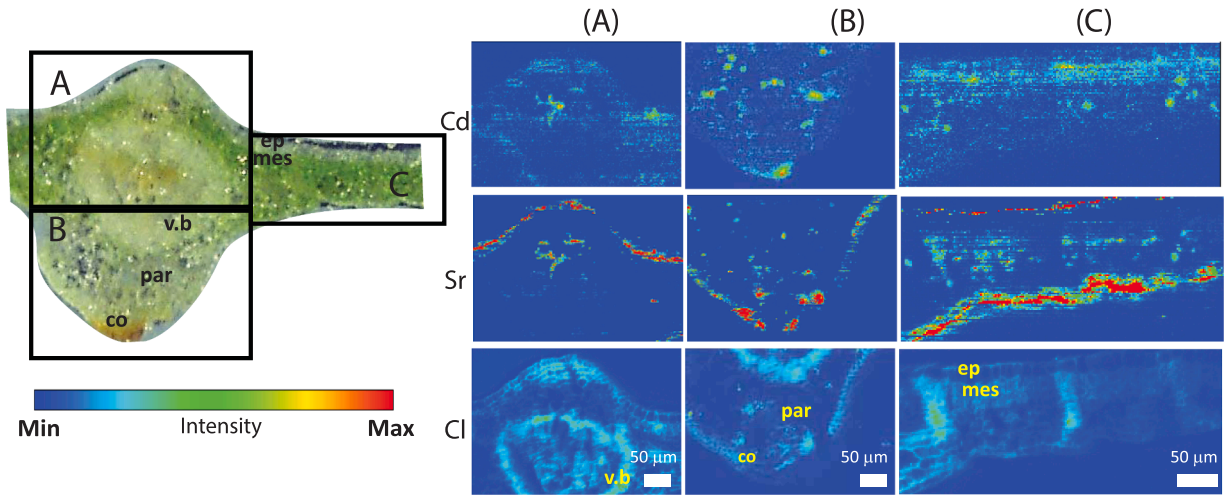

Fig. 4. Optical image of a secondary vein of a frozen-hydrated leaf of biological replicate T4 with the areas analysed with µXRF (rectangles A, B, and C). The heatmaps show the distribution of Cd, Sr, and Cl (pixel size: 1–2 µm). The color scale is adjusted to the range of each element (maximum photon counts: Cl: 10 000, Sr: 3000, Cd: 300). V.b: vascular bundle, ep: epidermis, mes: mesophyll, co: collenchyma, par: parenchyma. The Cl heatmaps are shown to visualize cellular structures. The Sr heatmaps are an indication for the presence of Ca-oxalate crystals. Cadmium was not detected in the vascular bundle (A). In the parenchymatous cells, there were local enrichments of Cd, some of which correlated with Sr, while others were primarily situated along cell walls (B). In the leaf blade, Cd was more abundant in the upper mesophyll than in the epidermis (C).

their strong co-localization with strontium (Sr) and calcium (Ca) (Fig. 2, S5, and S6). Calcium oxalate crystals were indeed previously observed in stems of *Theobroma cacao* (de Oliveira Ceita et al., 2007).

It is known that the incorporation of Sr in Ca-oxalate crystals is a common feature in plant cells (Kim and Heinrich, 1995). These crystals serve various critical functions in plants, such as regulating tissue calcium levels, providing a structural protection, deterring herbivory, fighting pathogen infections and facilitating metal detoxification (Franceschi and Nakata, 2005; Hawkesford et al., 2011; Nakata, 2003). To the best of our knowledge, Cd colocalization with Ca in crystals has only been reported for tobacco (*Nicotiana tabacum*) (Isaure et al., 2010), tomato (*Lycopersicon esculentum*) (Van Balen et al., 1980), water hyacinth (*Eichhornia crassipes*) (Mazen and El Maghraby, 1997) and the bioindicator *Gomphreni claussenii* (Pongrac et al., 2018; Villafort Carvalho et al., 2015). However, these studies had hydroponic setups with high (toxic) tissue Cd accumulation. This study is the first to show the incorporation of Cd in Ca-oxalate crystals at natural field Cd concentrations. The combined speciation measurements moreover revealed that the Cd in these crystals was mostly bound with O-ligands (Table 2, Fig. 5). This aligns with findings in *Gomphreni claussenii,* where the vast majority of Cd was bound to O-(C) ligands in oxalate crystals, which they suggested to be oxalate (Pongrac et al., 2018). The speciation measurements presented here are consistent with prior bulk Cd K-edge measurements conducted in mature branches, which indicated Cd binding to O-ligands (Blommaert et al., 2022). Yet, in previous study it was hypothesized that Cd was bound to vacuoles and cell-wall ligands, akin to observations in hyperaccumulator species (Cosio et al., 2005; Isaure et al., 2015; Sterckeman and Thomine, 2020; Vogel-Mikuš et al., 2010). The combination of imaging and speciation in this study gives a different perspective than the bulk speciation results, namely that Cd in branches is mostly bound to oxalate from Ca-oxalate crystals.

Part of Cd in the branches was present in non-crystalline structures (Fig. 1, 'z'). Here, Cd was bound to O-ligands, with S-ligands as minor species and correlated strongly with Mg (not shown). We identified this region as a large vessel structure. These vessels are possibly at the origin of big, lysigenous resin cavities in the pith of mature branches, which were previously identified to accumulate Cd (Blommaert et al., 2022). These resin channels are known to transport mucilage within the cacao tree (Brooks and Guard, 1952). Mucilage is a viscoelastic gel excreted by the plant, that contains mostly high-molecular-weight polysaccharides (Sasse et al., 2018). The mucilage surrounding the pulp of cacao beans has been shown to consist out of pectic polysaccharides (Alba et al., 2021; Meersman et al., 2017). Cadmium could possibly bind to the carboxyl/hydroxyl groups of these pectic polysaccharides (O-ligands). To the best of our knowledge, there are no studies that have identified the major components of mucilage in branches of *Theobroma cacao*. Yet, the imaging data in both mature and young branches suggest that mucilage may play a role in the transport and storage of Cd within cacao trees.

To summarize, our findings unveil calcium oxalate crystals as primary Cd storage structures within cacao branches. Cd has a high affinity for Ca-oxalate, and can be sorbed or incorporated in the crystals (McBride et al., 2017). Thus, this association of Cd with the crystal likely represents an efficient sequestration mechanism. At the contrary, the presence of Cd in in large vessels of the pith indicate some mobile form of Cd transported in the mucilage.

4.2. *Minor Cd retention in roots by binding with S-ligands and incorporation into Ca-oxalate crystals*

In our previous study (Blommaert et al., 2022), mass balance estimations indicated that only a small fraction of Cd was retained in roots, and that the majority of Cd was translocated to the shoot. In this study, our mapping analysis in the roots unveiled diverse Cd accumulation patterns and chemical forms (Fig. 3). Unlike the branches, there was no Cd detected in the periderm of the roots, corroborating that Cd is rapidly transported to the bark and wood for upward transport. Within the wood and bark regions of the roots, we once again observed the colocalization of Cd with calcium oxalate crystals and the dominant Cd speciation with O-ligands (Fig. 3, Table 2). However, the abundance of the crystals in the roots was lower compared to the branches, and even absent in one of the biological replicates. In the case of Cd-tolerant *Gomphrena Clausenii* (Pongrac et al., 2018), the roots did not contain oxalate crystals, despite the stems being rich in these crystals. Instead, the predominant binding of Cd in the roots of *Gomphrena Clausenii* was with S-ligands. Cadmium binding to thiols and vacuolar sequestration of these complexes is currently considered as one of the main detoxification mechanisms in non-hyperaccumulating plants (Leitenmaier and Küpper, 2013; Pons et al., 2021; Sterckeman and Thomine, 2020; Wiggenhauser et al., 2021 b).

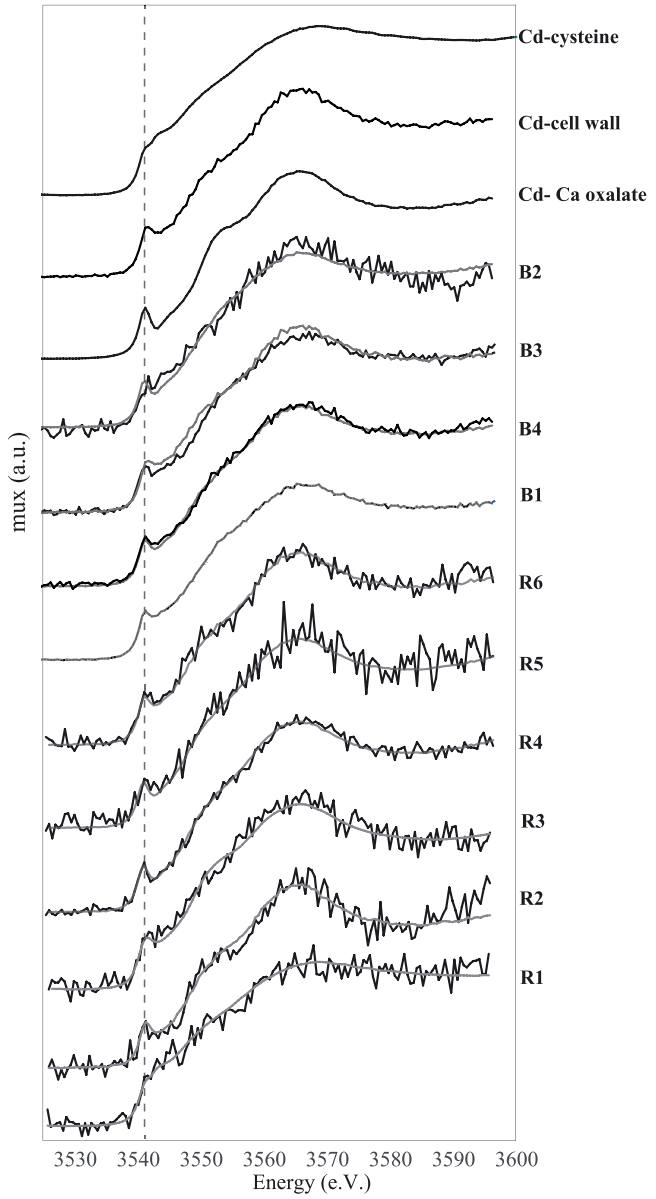

Fig. 5. Cd L_{III}-edge XANES spectra (black) and corresponding linear combination fits (LCFs, grey) of the Cd spots defined in Fig. 1 (B1, B2, B3, B4 in the branches) and Fig. 3 (R1, R2, R3, R4, R5, and R6 in the roots). LCF was performed by fitting the normalized XANES spectra in regions between −20 and 55 eV around the absorption edge, with the database of Cd reference compounds. We distinguished between two major groups of ligands that bind Cd in plants; (i) O-ligands represented by the references of Cd-cell wall, Cd-malate, Cd-oxalate, and Cd-pectin, S-ligands represented by the references Cd-cysteine and Cd-glutathione. The Cd L_{III}-edge XANES spectra show a clear distinction between Cd-S and Cd-O species because the Cd-O species have a peak at 3539 eV, indicated by the dashed vertical line.

It is thus remarkable that in cacao roots, the dominant form of Cd binding involves oxygen ligands. The complexation of Cd as Cd-O was previously observed in the roots of Cd hyperaccumulator plants (Tian et al., 2011; Vogel-Mikuš et al., 2010). The authors suggested that this complexation primarily occurs with cell-wall-O ligand components or small organic acids within vacuoles (Leitenmaier and Küpper, 2013; Sterckeman and Thomine, 2020). These oxygen ligands were thought to bind Cd relatively weakly compared to S-ligands, potentially facilitating its transport to aboveground tissues (Huguet et al., 2015; Küpper et al., 2004; Vogel-Mikuš et al., 2010). In our study, we also observed some Cd-S forms in the dilated cells of the wood near the cambium (R1). Yet,

Table 2
Results linear combination fits of Cd μXANES spectra combined with localization information determined by μXRF-analysis.

Spot	Location	Cd-species (%)		R-factor LCF (%)	Characteristic
		Cd-O	Cd-S		
B1	Big vessel	100	0	0.166	Strong colocalization with Mg
		60	40	0.161	
B2	Cambium	100	0	0.358	Ca-oxalate crystal
		55	45	0.347	
B3	Cambium	100	0	0.07	Ca-oxalate crystal
B4	Cambium	100	0	0.052	Ca-oxalate crystal
R1	Wood	0	100	0.048	No colocalization with elements measured
R2	Bark	85	15	0.281	Ca-oxalate crystal
		55	45	0.263	
R3	Wood	100	0	0.068	Ca-oxalate crystal
R4	Wood	100	0	0.097	No colocalization with elements measured
R5	Bark	100	0	0.760	Cambium
		85	15	0.784	
R6	Bark	100	0	0.259	S-rich spot

Spots are defined in μXRF images in Fig. 1 and Fig. 3 (B = branches, R = roots). The Cd L_{III}-edge XANES spectra of the Cd spots are shown in Fig. 5. The location depicts the structural regions defined in Figs. 1 and 3. We distinguished between two major group of species (i) Cd-O species (represented by Cd-cell wall, Cd-malate, Cd-oxalate, and Cd-pectin), and (ii) Cd-S species (represented by Cd-cysteine and Cd-glutathione). The R-factor (in %) ($= \sum[\mu_{exp} - \mu_{fit}]^2 / \sum[\mu_{exp}]^2$)*100 was used to assess the goodness of fit. If the R-factor increases <10 %, the fits are considered of equivalent quality.

our maps did not allow the localization of Cd within the cellular structures, it remains thus unclear if these Cd-S complexes reside within the vacuole or not, and if they contributed to Cd root sequestration.

Considering that most of the Cd in the cacao roots is being transported to the shoot (Blommaert et al., 2022; Engbersen et al., 2019), we suggest that in cacao roots, the majority of O-ligands are binding Cd relatively weakly, and that minor part of Cd is retained by binding with oxalate within calcium oxalate crystals or by binding with S-ligands.

4.3. Cadmium accumulates in the parenchyma, collenchyma, and mesophyll of the leaves

The measured Cd concentrations in the leaves of NA 312 were 3.49 ± 1.12 mg Cd kg^{-1} (mean ± SD, *n*=3 biological replicates) (Blommaert et al., 2022). This falls within the range of natural concentrations observed in various cacao plantations, with an average leaf Cd concentration of 2.6 mg kg^{-1} dry weight, as derived from a meta-analysis involving 762 samples (Vanderschueren et al., 2021). Cadmium in plant leaves is compartmentalized to reduce damage to important proteins, especially the ones involved in photosynthesis (Leitenmaier and Küpper, 2013). Hence, the Cd concentration is generally higher in the epidermis than in the mesophyll that contains photosynthesizing cells (Sterckeman and Thomine, 2020). However, our study showed the inverse, with an enrichment of Cd in the mesophyll versus the epidermis (Fig. 4 and S7). This phenomenon was also observed for Cd in the Zn hyperaccumulator *Arabidopsis halleri* (Isaure et al., 2015; Küpper et al., 2000; Leitenmaier and Küpper, 2013) and for *Sedum alfredii* (Tian et al., 2017). In the first-mentioned study, it was suggested that an enhanced storage in the mesophyll could be due to a saturation of the storage capacity of the epidermis (Küpper et al., 2000). The latter study proposed that Cd was rapidly transported into vacuoles of the parenchyma cells of the mesophyll for storage (Tian et al., 2017). Because our imaging data does not indicate a saturation of Cd in the epidermis (Fig. 4 and S7), we rather suggest that Cd is transported into vacuoles of the parenchyma cells of cacao in the mesophyll.

In willow, a woody species, Cd was accumulating in the collenchyma cell walls of the leaves (Vollenweider et al., 2011). Our study indicated that there was a Cd hotspot in the collenchyma (Fig. 4), but this was not as systematic as in the case of willow. Overall, Cd was more heterogeneously spread throughout the leaf tissues than in willow, where the Cd was more compartmentalized. The willow was nonetheless exposed to higher Cd concentrations. The Ca-oxalate crystals that were abundant in the roots and branches in the high Cd accumulator were again observed in the leaves (Figure S7). Yet, there was no Sr (and Ca)-Cd co-localization like observed in the branches and roots. Regulation of Cd through incorporation into the Ca-oxalate crystals played thus a minor role in the cacao leaves compared to the roots and branches in this study. The absence of Cd in the phloem in our study suggested that at the time of sampling, the Cd reallocation from leaves to other organs through phloem was limited.

5. Conclusions

In conclusion, our research revealed distinct Cd accumulation patterns within different plant organs and their tissues in a high Cd accumulating genotype of *Theobroma cacao* L. (NA 312). Notably, we found a prevalence of Cd-O species in the roots and branches, which contrasts with the typical Cd-S species observed in non-tolerant species. This phenomenon might be attributed to different Cd accumulation mechanisms present in cacao, and the reduced synthesis of S-ligands for Cd detoxification at background Cd concentrations compared to the studies that had higher Cd exposure. An important highlight of our study is the first-time observation of Cd incorporation into calcium oxalate crystals at natural field Cd concentrations in both roots and branches, with branches showing the highest abundance of these crystals. Although calcium oxalate crystals were also detected in leaves, they did not play a role in Cd detoxification in the leaves.

The strength of this study is that it is one of the first to study Cd speciation and distribution at natural, background Cd concentrations in a perennial crop. Yet, this study was limited to one cultivar and the examination of only two biological replicates due to the challenges and long acquisition times associated with measurements at background Cd concentrations. Further research with diverse genotypes and environmental conditions would strengthen these findings and provide a broader perspective on Cd accumulation in cacao plants. In broader terms, the implication of this study is that the mechanisms governing Cd storage and translocation in cacao plants (a moderate Cd accumulator) at background Cd concentrations, diverge from those observed in non-tolerant species such as cereals.

Funding

This work was financially supported by the French National Research Agency program 'Investissements d'avenir' (ANR-15-IDEX-02), the CNRS/INSU/EC2CO project CACAO, and the LabEx OSUG - AO International Bis 2021 project CACAO. HB and GS (ISTerre) are part of Labex OSUG (ANR10 LABX56). GS, HB and ES are working in the framework of the Program Hubert Curien "TOURNESOL" 2020–2021 (project n° 44274TC). HB, HC-M, ES, and GS are members of the COST Action CA19116 PLANTMETALS (COST, European Cooperation in Science and Technology, www.cost.eu).

CRediT authorship contribution statement

Géraldine Sarret: Writing – review & editing, Validation, Supervision, Project administration, Methodology, Investigation, Funding acquisition, Formal analysis, Data curation, Conceptualization. **Giulia Veronesi:** Writing – review & editing, Methodology, Investigation, Formal analysis, Data curation. **Rémi Tucoulou:** Writing – review & editing, Methodology. **Hester Blommaert:** Writing – original draft, Visualization, Software, Methodology, Investigation, Formal analysis, Data curation, Conceptualization. **Hiram Castillo-Michel:** Writing – review & editing, Visualization, Validation, Software, Methodology, Investigation, Formal analysis, Data curation, Conceptualization. **Jacques Beauchêne:** Writing – review & editing, Investigation. **Pathmanathan Umaharan:** Writing – review & editing, Resources, Methodology, Investigation, Formal analysis, Conceptualization. **Erik Smolders:** Writing – review & editing, Validation, Supervision, Resources, Methodology, Investigation, Conceptualization.

Declaration of Competing Interest

No conflict of interest declared.

Acknowledgements

We express our gratitude to the entire staff of the Cocoa Research Centre for the help with the collection of samples. We thank the staff of the Geochemistry Mineralogy Platform at ISTerre and KULeuven for their laboratory support. We acknowledge the review committees for the provision of beamtime at ID16b and ID21 (ESRF) and we thank the beamline staff on both beamlines for their help during measurement, especially Eduardo Villalobos-Portillo.

Appendix A. Supporting information

Supplementary data associated with this article can be found in the online version at doi:10.1016/j.envexpbot.2024.105713.

References

Alba, K., Nguyen, P.T.M., Kontogiorgos, V., 2021. Sustainable polysaccharides from Malvaceae family: structure and functionality. Food Hydrocoll. 118, 106749 https://doi.org/10.1016/j.foodhyd.2021.106749.

Angyalossy, V., Pace, M.R., Evert, R.F., Marcati, C.R., Oskolski, A.A., Terrazas, T., Kotina, E., Lens, F., Mazzoni, S.C., Angeles, G., MacHado, S.R., Crivellaro, A., Rao, K. S., Junikka, L., Nikolaeva, N., Baas, P., 2016. IAWA List of Microscopic Bark Features. IAWA J. 37, 517–615. https://doi.org/10.1163/22941932-20160151.

Aucour, A.M., Sarret, G., Blommaert, H., Wiggenhauser, M., 2023. Coupling metal stable isotope compositions and X-ray absorption spectroscopy to study metal pathways in soil-plant systems: a mini review. Metallomics, mfad016. https://doi.org/10.1093/mtomcs/mfad016.

Australia New Zealand Food Standards Code, 2017. Schedule 19 Maximum levels of contaminants and natural toxicants.

Blommaert, H., Aucour, A., Wiggenhauser, M., Moens, C., Telouk, P., Landrot, G., Testemale, D., Pin, S., Lewis, C., Umaharan, P., Smolders, E., Sarret, G., 2022. From soil to cacao bean: Unravelling the pathways of cadmium translocation in a high Cd accumulating cultivar of Theobroma cacao L. Front. Plant Sci. 1–19. https://doi.org/10.3389/fpls.2022.1055912.

Brooks, E., Guard, A., 1952. Vegetative Anatomy of Theobroma cacao. Bot. Gaz. 113, 444–454. https://doi.org/10.1017/CBO9781107415324.004.

Castillo-michel, H., Larue, C., Pradas del Real, A., Cotte, M., Sarret, G., 2017. Practical review on the use of synchrotron based micro- and nano- X-ray fluorescence mapping and X-ray absorption spectroscopy to investigate the interactions between plants and engineered nanomaterials. Plant Physiol. Biochem. 110, 13–32. https://doi.org/10.1016/j.plaphy.2016.07.018.

Clemens, S., 2019. Metal ligands in micronutrient acquisition and homeostasis. Plant Cell Environ. 42, 2902–2912. https://doi.org/10.1111/pce.13627.

Clemens, S., Ma, J.F., 2016. Toxic heavy metal and metalloid accumulation in crop plants and foods. Annu. Rev. Plant Biol. 67, 489–512. https://doi.org/10.1146/annurev-arplant-043015-112301.

Codex Alimentarius Commission, 2018. Report of the 12th session of the codex committee on contaminants in foods. Utrecht, The Netherlands.

Cosio, C., DeSantis, L., Frey, B., Diallo, S., Keller, C., 2005. Distribution of cadmium in leaves of Thlaspi caerulescens. J. Exp. Bot. 56, 765–775. https://doi.org/10.1093/jxb/eri062.

Cotte, M., Pouyet, E., Salomé, M., Rivard, C., De Nolf, W., Castillo-Michel, H., Fabris, T., Monico, L., Janssens, K., Wang, T., Sciau, P., Verger, L., Cormier, L., Dargaud, O., Brun, E., Bugnazet, D., Fayard, B., Hesse, B., Pradas Del Real, A.E., Veronesi, G., Langlois, J., Balcar, N., Vandenberghe, Y., Solé, V.A., Kieffer, J., Barrett, R., Cohen, C., Cornu, C., Baker, R., Gagliardini, E., Papillon, E., Susini, J., 2017. The ID21 X-ray and infrared microscopy beamline at the ESRF: status and recent applications to artistic materials. J. Anal. At. Spectrom. 32, 477–493. https://doi.org/10.1039/c6ja00356g.

de Oliveira Ceita, G., Macêdo, J.N.A., Santos, T.B., Alemanno, L., da Silva Gesteira, A., Micheli, F., Mariano, A.C., Gramacho, K.P., da Costa Silva, D., Meinhardt, L., Mazzafera, P., Pereira, G.A.G., de Mattos Cascardo, J.C., 2007. Involvement of calcium oxalate degradation during programmed cell death in Theobroma cacao

tissues triggered by the hemibiotrophic fungus Moniliophthora perniciosa. Plant Sci. 173, 106–117. https://doi.org/10.1016/j.plantsci.2007.04.006.
Demšar, J., Curk, T., Erjavec, A., Gorup, Č., Hočevar, T., Milutinovič, M., Možina, M., Polajnar, M., Toplak, M., Starič, A., Štajdohar, M., Umek, L., Žagar, L., Žbontar, J., Žitnik, M., Zupan, B., 2013. Orange: data mining toolbox in python. J. Mach. Learn. Res. 14, 2349–2353.
Engbersen, N., Gramlich, A., Lopez, M., Schwarz, G., Hattendorf, B., Gutierrez, O., Schulin, R., 2019. Cadmium accumulation and allocation in different cacao cultivars. Sci. Total Environ. 678, 660–670. https://doi.org/10.1016/j.scitotenv.2019.05.001.
EU, 2014. COMMISSION REGULATION (EU) No 488/2014 of 12 May 2014 amending Regulation (EC) No 1881/2006 as regards maximum levels of cadmium in foodstuffs. Off. J. Eur. Union 9. https://doi.org/10.2903/j.efsa.2011.1975.
FAO/WHO, 2010. Evaluation of certain food additives and contaminants: Seventy-third report of the joint FAO/WHO Expert Committee on Food Additives, WHO technical report series no. 960.
Franceschi, V.R., Nakata, P.A., 2005. Calcium oxalate in plants: Formation and function. Annu. Rev. Plant Biol. 56, 41–71. https://doi.org/10.1146/annurev.arplant.56.032604.144106.
Gu, Y., Wang, P., Zhang, S., Dai, J., Chen, H.P., Lombi, E., Howard, D.L., Van Der Ent, A., Zhao, F.J., Kopittke, P.M., 2020. Chemical speciation and distribution of cadmium in rice grain and implications for bioavailability to humans. Environ. Sci. Technol. 54, 12072–12080. https://doi.org/10.1021/acs.est.0c03001.
Hawkesford, M., Horst, W., Kichey, T., Lambers, H., Schjoerring, J., Møller, I.S., White, P., 2011. Functions of Macronutrients, Marschner's Mineral Nutrition of Higher Plants, Third Edition. Elsevier Ltd. https://doi.org/10.1016/B978-0-12-384905-2.00006-6
Huguet, S., Bert, V., Laboudigue, A., Barthès, V., Isaure, M.P., Llorens, I., Schat, H., Sarret, G., 2012. Cd speciation and localization in the hyperaccumulator Arabidopsis halleri. Environ. Exp. Bot. 82, 54–65. https://doi.org/10.1016/j.envexpbot.2012.03.011.
Huguet, S., Isaure, M.P., Bert, V., Laboudigue, A., Proux, O., Flank, A.M., Vantelon, D., Sarret, G., 2015. Fate of cadmium in the rhizosphere of Arabidopsis halleri grown in a contaminated dredged sediment. Sci. Total Environ. 536, 468–480. https://doi.org/10.1016/j.scitotenv.2015.07.026.
Isaure, M.-P., Sarret, G., Harada, E., Choi, Y.-E., Marcus, M.A., Fakra, S.C., Geoffroy, N., Pairis, S., Susini, J., Clemens, S., Manceau, A., 2010. Calcium promotes cadmium elimination as vaterite grains by tobacco trichomes. Geochim. Cosmochim. Acta 74, 5817–5834. https://doi.org/10.1016/j.gca.2010.07.011.
Isaure, M.P., Fayard, B., Sarret, G., Pairis, S., Bourguignon, J., 2006. Localization and chemical forms of cadmium in plant samples by combining analytical electron microscopy and X-ray spectromicroscopy. Spectrochim. Acta - Part B . Spectrosc. 61, 1242–1252. https://doi.org/10.1016/j.sab.2006.10.009.
Isaure, M.P., Huguet, S., Meyer, C.L., Castillo-Michel, H., Testemale, D., Vantelon, D., Saumitou-Laprade, P., Verbruggen, N., Sarret, G., 2015. Evidence of various mechanisms of Cd sequestration in the hyperaccumulator Arabidopsis halleri, the non-accumulator Arabidopsis lyrata, and their progenies by combined synchrotron-based techniques. J. Exp. Bot. 66, 3201–3214. https://doi.org/10.1093/jxb/erv131.
Kim, T.W., Heinrich, G., 1995. Use of a laser microprobe mass analyzer for detection of strontium incorporation in oxalate-crystals of beta vulgaris leaf. J. Plant Physiol. 146, 217–221. https://doi.org/10.1016/S0176-1617(11)82044-4.
Kopittke, P.M., Punshon, T., Paterson, D.J., Tappero, R.V., Wang, P., Blamey, F.P.C., van der Ent, A., Lombi, E., 2018. Synchrotron-based X-ray fluorescence microscopy as a technique for imaging of elements in plants. Plant Physiol. 178, 507–523. https://doi.org/10.1104/pp.18.00759.
Küpper, H., Lombi, E., Zhao, F., Mcgrath, S.P., 2000. Cellular compartmentation of cadmium and zinc in relation to other elements in the hyperaccumulator Arabidopsis halleri. Planta 212, 75–84. https://doi.org/10.1007/s004250000366.
Küpper, H., Mijovilovich, A., Meyer-Klaucke, W., Kroneck, P.M.H., 2004. Tissue- and age-dependent differences in the complexation of cadmium and zinc in the cadmium/zinc hyperaccumulator thlaspi caerulescens (ganges ecotype) revealed by X-ray absorption spectroscopy. Plant Physiol. 134, 748–757. https://doi.org/10.1104/pp.103.032953.
Landrot, G., 2018. FASTOSH: A Software to Process XAFS Data for Geochemical & Environmental Applications, in: Goldschmidt Abstracts. Boston.
Leitenmaier, B., Küpper, H., 2013. Compartmentation and complexation of metals in hyperaccumulator plants. Front. Plant Sci. 4, 1–13. https://doi.org/10.3389/fpls.2013.00374.
Lewis, C., Lennon, A.M., Eudoxie, G., Umaharan, P., 2018. Genetic variation in bioaccumulation and partitioning of cadmium in Theobroma cacao L. Sci. Total Environ. 640–641, 696–703. https://doi.org/10.1016/j.scitotenv.2018.05.365.
Mazen, A.M.A., El Maghraby, O.M.O., 1997. Accumulation of cadmium, lead and strontium, and a role of calcium oxalate in water hyacinth tolerance. Biol. Plant. 40, 411–417. https://doi.org/10.1023/A:1001174132428.
McBride, M.B., Frenchmeyer, M., Kelch, S.E., Aristilde, L., 2017. Solubility, structure, and morphology in the co-precipitation of cadmium and zinc with calcium-oxalate. J. Colloid Interface Sci. 486, 309–315. https://doi.org/10.1016/j.jcis.2016.09.079.
McLaughlin, M.J., Smolders, E., Zhao, F.J., Grant, C., Montalvo, D., 2021. In: D.L.B.T.-A. in A. (Ed.), Chapter One - Managing cadmium in agricultural systems, in: Sparks. Academic Press, pp. 1–129. https://doi.org/10.1016/bs.agron.2020.10.004.
Meersman, E., Struyf, N., Kyomugasho, C., Jamsazzadeh Kermani, Z., Santiago, J.S., Baert, E., Hemdane, S., Vrancken, G., Verstrepen, K.J., Courtin, C.M., Hendrickx, M., Steensels, J., 2017. Characterization and Degradation of Pectic Polysaccharides in Cocoa Pulp. J. Agric. Food Chem. 65, 9726–9734. https://doi.org/10.1021/acs.jafc.7b03854.
Mercosur, 2011. Reglamento técnico Mercosur sobre límites máximos de contaminantes inorgánicos en alimentos (Derogación De Las Res. GMC N° 102/94 y N° 36/96).
Meter, A., Atkinson, R.J., Laliberte, B., 2019. Cadmium in Cacao from Latin America and the Carribean. A Review of Research and Potential Mitigation Solutions. Bioversity International, Rome. https://doi.org/10.1017/CBO9781107415324.004.
Ministry of Health of the Russian Federation, 2011. Chief State Sanitary Inspector of the Russian Federation Resolution no. 36 - On Enactment of Sanitary Rules.
Motamayor, J.C., Lachenaud, P., da Silva e Mota, J.W., Loor, R., Kuhn, D.N., Brown, J.S., Schnell, R.J., 2008. Geographic and genetic population differentiation of the Amazonian chocolate tree (Theobroma cacao L). PLoS One 3. https://doi.org/10.1371/journal.pone.0003311.
Nakata, P.A., 2003. Advances in our understanding of calcium oxalate crystal formation and function in plants. Plant Sci. 164, 901–909. https://doi.org/10.1016/S0168-9452(03)00120-1.
Page, V., Feller, U., 2015. Heavy metals in crop plants: Transport and redistribution processes on the whole plant level. Agronomy 5, 447–463. https://doi.org/10.3390/agronomy5030447.
Pickering, I.J., Prince, R.C., George, G.N., Rauser, W.E., Wickramasinghe, W.A., Watson, A.A., Dameron, C.T., Dance, I.G., Fairlie, D.P., Salt, D.E., 1999. X-ray absorption spectroscopy of cadmium phytochelatin and model systems. Biochim. Biophys. Acta - Protein Struct. Mol. Enzymol. 1429, 351–364. https://doi.org/10.1016/S0167-4838(98)00242-8.
Pongrac, P., Serra, T.S., Castillo-Michel, H., Vogel-Mikuš, K., Arčon, I., Kelemen, M., Jenčič, B., Kavčič, A., Villafort Carvalho, M.T., Aarts, M.G.M., 2018. Cadmium associates with oxalate in calcium oxalate crystals and competes with calcium for translocation to stems in the cadmium bioindicator Gomphrena claussenii. Metallomics 10, 1576–1584. https://doi.org/10.1039/c8mt00149a.
Pons, M.L., Collin, B., Doelsch, E., Chaurand, P., Fehlauer, T., Levard, C., Keller, C., Rose, J., 2021. X-ray absorption spectroscopy evidence of sulfur-bound cadmium in the Cd-hyperaccumulator Solanum nigrum and the non-accumulator Solanum melongena. Environ. Pollut. 279 https://doi.org/10.1016/j.envpol.2021.116897.
Sari, S.H.J., Chien, M.F., Inoue, C., 2022. Subcellular localization and chemical speciation of Cd in Arabidopsis halleri ssp. gemmifera to reveal its hyperaccumulating and detoxification strategies. Environ. Exp. Bot. 203, 105047 https://doi.org/10.1016/j.envexpbot.2022.105047.
Sarret, G., Smits, E.A.H.P., Michel, H.C., Isaure, M.P., Zhao, F.J., Tappero, R., 2013. Use of synchrotron-based techniques to elucidate metal uptake and metabolism in plants. In: Advances in Agronomy. Elsevier, pp. 1–82. https://doi.org/10.1016/B978-0-12-407247-3.00001-9.
Sasse, J., Martinoia, E., Northen, T., 2018. Feed Your Friends: Do Plant Exudates Shape the Root Microbiome? Trends Plant Sci. 23, 25–41. https://doi.org/10.1016/j.tplants.2017.09.003.
Sigel, A., Sigel, H., Sigel, R.K.O., 2013. Cadmium: From Toxicity to Essentiality, Cadmium: From Toxicity to Essentiality. Springer. https://doi.org/10.1007/978-94-007-5179-8.
Smolders, E., Mertens, J., 2013. Cadmium. In: Heavy Metals in Soils: Trace Metals and Metalloids in Soils 283 and Their Bioavailability. Springer, Dordrecht, pp. 283–308. https://doi.org/10.1007/978-94-007-4470-7.
Sterckeman, T., Thomine, S., 2020. Mechanisms of Cadmium Accumulation in Plants. CRC Crit. Rev. Plant Sci. 39, 322–359. https://doi.org/10.1080/07352689.2020.1792179.
Tian, S., Lu, L., Labavitch, J., Yang, X., He, Z., Hu, H., Sarangi, R., Newville, M., Commisso, J., Brown, P., 2011. Cellular sequestration of cadmium in the hyperaccumulator plant species Sedum alfredii. Plant Physiol. 157, 1914–1925. https://doi.org/10.1104/pp.111.183947.
Tian, S., Xie, R., Wang, H., Hu, Y., Hou, D., Liao, X., Brown, P.H., Yang, H., Lin, X., Labavitch, J.M., Lu, L., 2017. Uptake, sequestration and tolerance of cadmium at cellular levels in the hyperaccumulator plant species Sedum alfredii. J. Exp. Bot. 68, 2387–2398. https://doi.org/10.1093/jxb/erx112.
Van Balen, E., Van De Geijn, S.C., Desmet, G.M., 1980. Autoradiographic evidence for the incorporation of cadmium into calcium oxalate crystals. Z. Pflanzenphysiol. 97, 123–133. https://doi.org/10.1016/s0044-328x(80)80026-2.
van der Ent, A., Baker, A.J.M., Reeves, R.D., Pollard, A.J., Schat, H., 2013. Hyperaccumulators of metal and metalloid trace elements: Facts and fiction. Plant Soil 362, 319–334. https://doi.org/10.1007/s11104-012-1287-3.
van der Ent, A., Przybyłowicz, W.J., de Jonge, M.D., Harris, H.H., Ryan, C.G., Tylko, G., Paterson, D.J., Barnabas, A.D., Kopittke, P.M., Mesjasz-Przybyłowicz, J., 2018. X-ray elemental mapping techniques for elucidating the ecophysiology of hyperaccumulator plants. New Phytol. 218, 432–452. https://doi.org/10.1111/nph.14810.
Vanderschueren, R., Argüello, D., Blommaert, H., Montalvo, D., Barraza, F., Maurice, L., Schreck, E., Schulin, R., Lewis, C., Vazquez, J.L., Umaharan, P., Chavez, E., Sarret, G., Smolders, E., 2021. Mitigating the level of cadmium in cacao products: Reviewing the transfer of cadmium from soil to chocolate bar. Sci. Total Environ. 781, 146779 https://doi.org/10.1016/j.scitotenv.2021.146779.
Viet, Ha, L.T., Hang, P.T., Everaert, H., Rottiers, H., Anh, L.P.T., Dung, T.N., Phuoc, P.H. D., Toan, H.T., Dewettinck, K., Messens, K., 2016. Characterization of leaf, flower, and pod morphology among vietnamese cocoa varieties (Theobroma cacao L.). Pak. J. Bot. 48, 2375–2383.
Villafort Carvalho, M.T., Pongrac, P., Mumm, R., van Arkel, J., van Aelst, A., Jeromel, L., Vavpetič, P., Pelicon, P., Aarts, M.G.M., 2015. Gomphrena claussenii, a novel metal-hypertolerant bioindicator species, sequesters cadmium, but not zinc, in vacuolar oxalate crystals. New Phytol. 208, 763–775. https://doi.org/10.1111/nph.13500.
Vogel-Mikuš, K., Arčon, I., Kodre, A., 2010. Complexation of cadmium in seeds and vegetative tissues of the cadmium hyperaccumulator Thlaspi praecox as studied by X-ray absorption spectroscopy. Plant Soil 331, 439–451. https://doi.org/10.1007/s11104-009-0264-y.

Vollenweider, P., Menard, T., Günthardt-Goerg, M.S., 2011. Compartmentation of metals in foliage of Populus tremula grown on soils with mixed contamination. I. from the tree crown to leaf cell level. Environ. Pollut. 159, 324–336. https://doi.org/10.1016/j.envpol.2010.07.013.

White, P.J., Ding, G., 2023. Chapter 3 - Long-distance transport in the xylem and phloem. In: Rengel, Z., Cakmak, I., White, P.J.B.T.-M.M.N., of P. (Fourth E. (Eds.) (Eds.), Marschner's Mineral Nutrition of Higher Plants: Fourth Edition. Academic Press, San Diego, pp. 73–104. https://doi.org/10.1016/B978-0-12-819773-8.00002-2.

Wiggenhauser, M., Aucour, A., Telouk, P., Blommaert, H., Sarret, G., 2021a. Changes of cadmium storage forms and isotope ratios in rice during grain filling. Front. Plant Sci. 12, 1–18. https://doi.org/10.3389/fpls.2021.645150.

Wiggenhauser, M., Aucour, A.M., Bureau, S., Campillo, S., Telouk, P., Romani, M., Ma, J. F., Landrot, G., Sarret, G., 2021b. Cadmium transfer in contaminated soil-rice systems: Insights from solid-state speciation analysis and stable isotope fractionation. Environ. Pollut. 269 https://doi.org/10.1016/j.envpol.2020.115934.

Yan, B., Isaure, M.P., Mounicou, S., Castillo-Michel, H., De Nolf, W., Nguyen, C., Cornu, J.Y., 2020. Cadmium distribution in mature durum wheat grains using dissection, laser ablation-ICP-MS and synchrotron techniques. Environ. Pollut. 260 https://doi.org/10.1016/j.envpol.2020.113987.

Yan, J., Tang, Z., Fischel, M., Wang, P., Siebecker, M.G., Aarts, M.G.M., Sparks, D.L., Zhao, F.J., 2022. Variation in cadmium accumulation and speciation within the same population of the hyperaccumulator Noccaea caerulescens grown in a moderately contaminated soil. Plant Soil 475, 379–394. https://doi.org/10.1007/s11104-022-05373-w.

Zhao, F.J., Moore, K.L., Lombi, E., Zhu, Y.G., 2014. Imaging element distribution and speciation in plant cells. Trends Plant Sci. 19, 183–192. https://doi.org/10.1016/j.tplants.2013.12.001.